Int. J. Heat Mass Transfer. Vol. 36, No. 4, pp. 989–997, 1993
Printed in Great Britain

0017–9310/93 $6.00 + 0.00

Air jet impingement heat transfer from modified surfaces

L. G. HANSEN and B. W. WEBB
Heat Transfer Laboratory, Brigham Young University, Provo, UT 84602, U.S.A.

(*Received* 6 *December* 1991 *and in final form* 17 *April* 1992)

Abstract—Experiments were performed to characterize heat transfer to a normally impinging air jet from surfaces modified with arrays of fin-type extensions. Heat transfer enhancement for six fin geometries was evaluated by comparison with results for a smooth, flat surface. Average Nusselt numbers ($\bar{Nu}$) and overall system effectiveness (ε) are reported as functions of fin type, jet Reynolds number (Re), and nozzle-to-plate spacing (z/d) for two nozzle diameters. Enhancement of the absolute rate of heat transfer, as compared to the smooth surface, was demonstrated by a factor ranging from 1.5 to 4.5. The system effectiveness as a function of Re exhibited strong fin type dependence due to significant variations in the total surface area and average Nusselt number. The fin type dependence of $\bar{Nu}$ as a function of Re was found to be a result of variations in the turbulence level, fluid velocity, and the percentages of total surface area exposed to normal, oblique, and parallel flow. The average Nusselt number correlated well in the form $\bar{Nu} = A\,Re^{m}$. For the modified surfaces, the system effectiveness decreased monotonically with increasing z/d in contrast to the smooth surface behavior.

INTRODUCTION

JET IMPINGEMENT is a common method of heating or cooling solid surfaces. Heat transfer under impinging jets is generally superior to that achieved with conventional methods of convective transport. Thus, most practical applications of jet impingement occur in industries where the heat transfer requirements have exceeded the capacity of ordinary heating and cooling techniques. Examples of industrial jet impingement include drying paper and textiles, tempering glass, annealing metals, and cooling gas turbine blades and electronic components.

The body of impinging jet literature is large. Most early work concentrated on jets impinging on smooth, flat surfaces [1, 2]. Jet impingement on smooth, curved surfaces also has been investigated [3]. More recently, jets impinging on arrays of blocks mounted on otherwise flat surfaces (simulated electronic packages) have attracted considerable attention [4, 5]. A number of investigators have observed that the relatively high heat transfer characteristic of impinging jets is related to high turbulence levels in the fluid flow [6–11]. A variety of turbulence promoting schemes have been used to enhance jet impingement heat transfer with varying degrees of success [2]. Of the previous reviews of jet impingement heat transfer work [2, 12–14], the most recent review noted the potential of combining extended surfaces with impinging jets, and a lack of research in this area [2]. The few investigations of jet impingement combined with extended surfaces have reported generally promising results. Ali Khan *et al.* [15] positioned a punched plate with circular holes upstream of a heated surface. Hrycak [16] studied heat transfer for a jet impinging on a smooth plate modified with spike and concentric ring protuberances. Obot and Trabold [17] investigated arrays of jets impinging on surfaces having repeated square ribs with transverse flow of the spent air. Fleishman and Yuen [18] utilized a wire screen mesh in a channel formed between two plates. The plates constrained the flow of an impinging, water jet through the channel. All of these studies revealed augmentation of the total heat transfer after the addition of surface modifications in the impinging jet region.

The foregoing studies indicate that significant enhancements in jet impingement heat transfer may be achieved with extended surfaces. The present study serves to further investigate this potential and the mechanisms of enhancement. An experimental investigation is reported of heat transfer to an axisymmetric impinging air jet for heated surfaces modified with arrays of extended surfaces. Heat transfer enhancement is evaluated by comparing the modified surface results to those obtained for a smooth, flat surface.

EXPERIMENTS

Apparatus

Figure 1 is a schematic of the experimental apparatus, which consists of a metered air supply, a jet nozzle, a heater assembly including the test surface, and the data acquisition and power supply equipment. The apparatus was designed to allow determination of average heat transfer coefficients for the heated test surface cooled with air impinging from the nozzle. Heat transfer coefficients were calculated from measurements of electrical power dissipated in the heater assembly, the average test surface base temperature, and the freestream air temperature.

Air was supplied from a large capacity tank,

NOMENCLATURE

A_b	exposed base area of a modified surface	P	perimeter of a fin
A_c	cross-sectional area of a fin	q	total heat transfer dissipated from the test surface
A_t	total heat transfer surface area	R	radius of test surface
$A_{t,s}$	total heat transfer surface area for the smooth surface	Re	jet Reynolds number, Vd/ν
d	jet nozzle diameter	T_s	test surface base temperature
H	fin height	T_∞	jet air temperature
$\bar{h}$	average heat transfer coefficient	u'	r.m.s. velocity fluctuation
k_a	thermal conductivity of air at film temperature	$\bar{u}$	radial component of average velocity
k_f	thermal conductivity of fins	V	average jet velocity
n	number of fins on a surface	y	normal distance from the test surface base
$\overline{Nu}$	average Nusselt number based on jet diameter, $\bar{h}d/k_a$	z	nozzle-to-plate spacing.
$\overline{Nu}_l$	average Nusselt number for the large nozzle	Greek symbols	
$\overline{Nu}_s$	average Nusselt number for the small nozzle	ε	overall system effectiveness
		ν	kinematic viscosity.

pressurized by an automatic shutoff air compressor. The air flowed from the tank through a pressure regulator, valve, filter, rotameter, and finally, the nozzle. The jet air temperature was measured at the nozzle inlet. Air properties were evaluated at the film temperature, the average of the surface temperature (T_s) and the jet air temperature at the nozzle inlet (T_∞).

Aluminum tubes of inside diameter 6.91 and 13.3

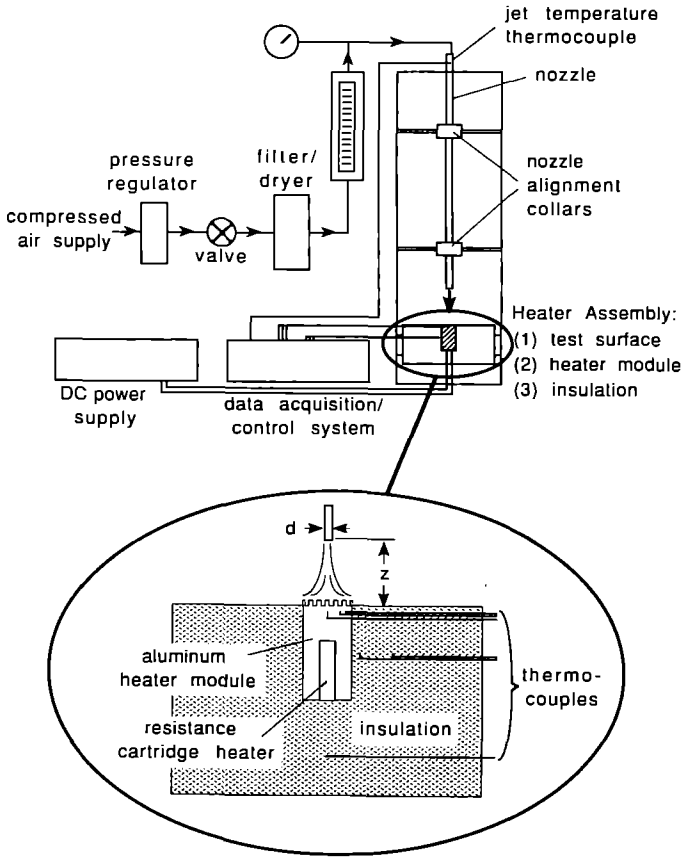

FIG. 1. Schematic of test apparatus and heater assembly.

mm were used for nozzles. The tubes were 650 and 910 mm in length, respectively, which was sufficient to insure fully-developed flow. The tube ends were machined square. The nozzles were supported at two points in a manner that allowed variation of the nozzle-to-plate spacing (z/d) while maintaining the nozzle normal and centered in relation to the test surface.

The heater assembly consisted of a cylindrical, aluminum heater module embedded in closed-pore, polystyrene insulation (Fig. 1). A heater assembly was constructed for each test surface including the smooth reference surface. Without extended surfaces, each heater module was 50.8 mm in height and had a diameter of 19.1 mm. The underside of each module was bored to accept a 75 W resistive cartridge heater. The upper surface of the module served as the base of the test surface and was positioned flush with the surrounding insulation. The insulation was at least 63 mm thick in all directions. The same cartridge heater and HP 6030A power supply were used with each heater assembly.

The surface temperature was determined as the average reading of three thermocouples positioned 3.18 mm below the test surface and at the centerline, half-radius, and outer edge of each heater module. Variation in the three temperature readings was never more than 2% of the average temperature difference between the test surface and the air jet ($T_s - T_\infty$). The temperature drop from the measurement depth to the actual test surface base was estimated with a two-dimensional finite difference model developed specifically for the experimental apparatus. It was determined that this temperature drop was negligible in comparison to the temperature difference between the test surface and the air jet.

The finite difference model was also used to estimate conduction losses through the insulation which varied from 5 to 15% of the Ohmic dissipation in the cartridge heater. The conduction model predictions were validated with temperature measurements taken at four locations in the surrounding insulation: (1) 25.4 mm beneath the heater module on the centerline, and 25.4 mm beneath the surface at radial distances of (2) 3.18 mm, (3) 12.7 mm, and (4) 25.4 mm from the heater module perimeter (see Fig. 1). The heat transfer results presented here were corrected for these losses using the results of the finite difference model.

The extended surfaces were machined as integral parts of each cylindrical aluminum module and protruded beyond the base length. The surface modifications studied here are depicted in Fig. 2. Extended surface elements of three of the modified surfaces had a square cross-section (1.59 × 1.59 mm) and were 1.59, 3.18, and 4.76 mm in height, respectively. A fourth extended surface element consisted of a pyramid 1.59 mm tall with a square base 3.18 mm on a side. A fifth surface was modified with three concentric rings 1.59 mm wide and 1.59 mm tall with 1.59 mm spacings. The sixth extended surface element was an annular ring with a width of 3.18 mm and a height of 6.35 mm. The ratio of total surface area to the area of the smooth surface is given in Table 1 for each test surface.

All temperature data were obtained with an HP 3421A Data Acquistion/Control Unit reading copper–constantan (T-type) thermocouples. Electrical voltage and current data were recorded from the HP 6030A System Power Supply digital output and verified with concurrent readings from the HP 3421A. Measurements of the air velocity and turbulence at the surface were obtained with a laser-Doppler velocimeter. The LDV system used a 5 W argon ion laser and was operated in backscatter mode. Seeding was accomplished by atomizing a dissolved salt solution. Three-thousand instantaneous velocity measurements were used in determining the mean and fluctuating radial velocity as a function of height at a radial distance of one jet diameter from the test surface perimeter. Sufficient data were obtained to represent the flow field from the base to the tip of the fins for the pyramidal, short square, intermediate square, and tall square surfaces. The uncertainty of the velocimetry measurements is estimated to be 4%.

Data reduction

Data were obtained to report average heat transfer coefficient and system effectiveness results as a function of jet Reynolds number (Re) for all seven test surfaces. In addition, data were obtained as a function of nozzle-to-surface spacing (z/d) for the smooth surface and the surfaces modified with the tall square fins, the short square fins, and the pyramidal fins. All experiments were performed with both nozzle diameters.

Heat transfer results for each surface are presented in terms of an average Nusselt number, which is defined as

$$\overline{Nu} = \bar{h}d/k_a. \tag{1}$$

Note that the average Nusselt number is not indicative of total heat transfer rate from the fin/base system, but is a measure of the average heat transfer coefficient. For the smooth surface, the average heat transfer coefficient was determined from

$$\bar{h} = q/A_t(T_s - T_\infty) \tag{2}$$

where A_t for the smooth surface is $A_t = A_{t,s} = \pi R^2$. For the modified test surfaces (excluding the pyramidal surface), the average heat transfer coefficient was approximated from an iterative solution of an expression for the total heat transfer from the fin/base system:

$$q = \bar{h}A_b(T_s - T_\infty) + \sum_{i=1}^{n} M_i \frac{\sinh(m_iH) + (\bar{h}/m_iH)\cosh(m_iH)}{\cosh(m_iH) + (\bar{h}/m_iH)\sinh(m_iH)} \tag{3}$$

where

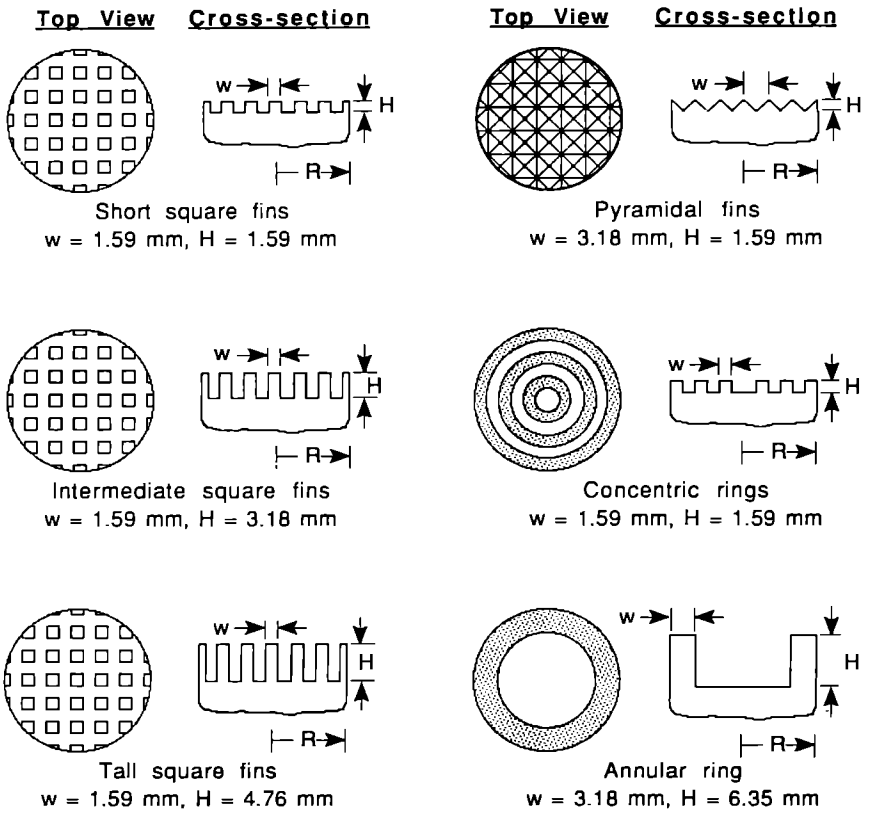

FIG. 2. Schematic of modified surfaces.

$$M_i = [\bar{h}P_i k_f A_{c,i}]^{1/2}(T_s - T_\infty) \quad (4)$$

and

$$m_i = \left[\frac{\bar{h}P_i}{k_f A_{c,i}}\right]^{1/2}. \quad (5)$$

The index, i, in the summation of equation (3) varies from 1 to n, the total number of fins on the test surface. Thus, the first term in equation (3) represents the heat transfer from the exposed base area, and the second term is the fin equation representing the heat transfer from the fins. For the short square, intermediate square, and tall square surfaces, the non-square cross-section of the fins on the test surface perimeter was accounted for through modification of the coefficients M_i and m_i.

Equation (3) does not apply for the pyramidal fins since the fin cross-sectional area (A_c) is not uniform. However, based on the fin system efficiency of the other modified surfaces, it was determined that equation (2) could be used for the pyramidal surface with less than a 1% increase in uncertainty. The efficiency for a given test surface is defined as the ratio of actual heat transfer from the fin to the heat transfer that would have occurred if the entire fin was at the test surface base temperature. The efficiency was determined to be greater than 0.99 for the short square finned surface, which is most similar to the pyramidal

Table 1. Ratio of the total surface area (A_t) to the smooth surface area ($A_{t,s}$) and the percentage of total surface area exposed to normal, oblique, and parallel flow

Surface	$A_{t,s}/A_s$	Normal (%)	Oblique (%)	Parallel (%)
Smooth	1.00	100	0	0
Pyramidal fins	1.55	0	100	0
Short square fins	2.13	47	0	53
Intermediate square fins	3.26	31	0	69
Tall square fins	4.39	23	0	77
Concentric rings	2.17			
Annular ring	3.22			

surface. The tall square surface had the lowest efficiency (greater than 0.95 for the worst case). Note that with such high fin efficiencies, the average heat transfer coefficient could have been determined by the approximate relation $q = \bar{h}A_t(T_s - T_\infty)$ for all modified surfaces.

Heat transfer enhancement for each extended surface geometry was evaluated in terms of an overall system effectiveness (ε), defined as the ratio of system heat transfer with extended surfaces to heat transfer without extended surfaces (for the same temperature difference):

$$\varepsilon = q_{\text{fin}}/q_{\text{smooth}}. \quad (6)$$

Equation (6) reflects the overall effectiveness of the fin/base system, and should not be confused with the effectiveness of the fins alone. While the average Nusselt number reflects the influence of surface modifications on average heat transfer coefficient, the overall system effectiveness illustrates the effect of modifications on total heat transfer from the fin/base system.

In order to determine average heat transfer coefficients the total heat transfer, q, and the temperature difference, $(T_s - T_\infty)$, were measured for each set of test conditions. The heat transfer was determined from the total electrical dissipation in the cartridge heaters. The electrical dissipation was calculated from Ohm's law using voltage and current measurements recorded during each test run. As mentioned previously, conduction losses were estimated with a two-dimensional finite difference model.

The temperature difference was found from measurements of the test surface temperature and the jet air temperature. After each change in test conditions, the voltage was adjusted to produce a steady-state temperature difference, $(T_s - T_\infty)$, of approximately 25°C. Convergence to steady-state conditions was monitored with temperature readings taken at five minute intervals. After reaching steady-state conditions (approximately 45 min), three complete sets of temperature readings were taken at five minute intervals and averaged temporally.

The maximum uncertainty in the average Nusselt numbers was estimated to be 7% [19]. The maximum uncertainty for jet Reynolds numbers was determined to be 6%, while the maximum uncertainty in the nozzle-to-plate spacing was estimated to be ± 0.5 mm.

RESULTS AND DISCUSSION

Experiments were performed for jet Reynolds numbers ranging from 4700 to 24000 for the small nozzle ($d = 6.91$ mm) and from 8100 to 33000 for the large nozzle ($d = 13.3$ mm). All Reynolds number parametric results were obtained for $z/d = 5$. The nozzle-to-plate spacing parametric study was performed from $z/d = 1/4$ to 14 with $Re = 14100$ for the small nozzle and $Re = 20400$ for the large nozzle. The results are presented in the following sections.

Reynolds number dependence

Figure 3 shows $\overline{Nu}$ as a function of Re for all surfaces studied. Results obtained with both nozzle diameters at $z/d = 5$ are shown. The results for the smooth surface were compared to previous work summarized by Martin [13]. (For the heated target–nozzle diameter ratios of $R/d = 0.71$ and 1.31 in this study, the graphical correlation of Martin was used, Fig. 9, ref. [13].) Agreement with the present experimental results is excellent; the average difference between the empirical correlation and experimental values is less than 4% for the small nozzle and less than 11% for the large nozzle.

The experimental results for all modified surfaces shown in Fig. 3 were correlated with an equation of the form

$$\overline{Nu} = A\,Re^m \quad (7)$$

where A and m are parameters determined with a least squares curve fit. The parameters A and m are shown in Table 2. Recall that $\overline{Nu}$ does not indicate total heat transfer but rather the average heat transfer coefficient over the fins and base. The R^2 measure of goodness of fit is greater than 0.996 for all data sets. While

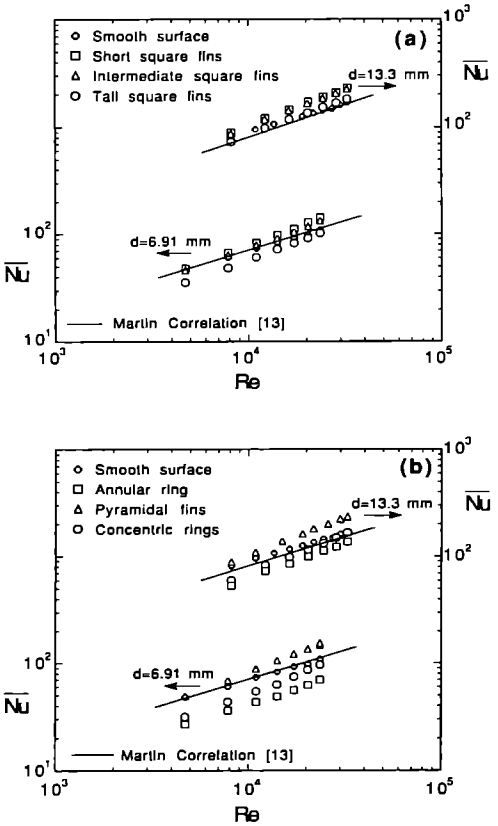

FIG. 3. Dependence of average Nusselt number on Reynolds number for all surfaces investigated, $z/d = 5$.

Table 2. Coefficients for the least-squares curve fit for equation (7)

Surface	$d = 6.91$ mm A	m	$d = 13.3$ mm A	m
Smooth	0.68	0.50	0.81	0.51
Pyramidal fins	0.13	0.70	0.16	0.70
Short square fins	0.16	0.67	0.22	0.67
Intermediate square fins	0.19	0.65	0.21	0.67
Tall square fins	0.14	0.65	0.21	0.65
Concentric rings	0.09	0.69	0.09	0.72
Annular ring	0.20	0.58	0.14	0.66

the smooth surface shows the conventional Nusselt number dependence on $Re^{1/2}$, heat transfer from the modified surfaces exhibits a stronger Reynolds number dependence, with the exponent on Re ranging from 0.58 to 0.72.

As seen in Fig. 3, the pyramidal, short square, and intermediate square fins result in enhanced $\overline{Nu}$, as compared to the smooth surface, for all test conditions. The largest increase is achieved with the pyramidal fins followed by the short square fins and then the intermediate fins. The tall square fins slightly enhance $\overline{Nu}$ for higher Re with the large nozzle and reduce $\overline{Nu}$ for all other test conditions. The concentric rings and annular ring reduce $\overline{Nu}$ for all conditions, with the annular ring having the most adverse effect.

As evident from these results, $\overline{Nu}$ is strongly dependent on fin type. As will be substantiated, this dependence is attributed to the interaction of three factors: (1) the level of turbulence, (2) the fluid velocity at the surface, and (3) the percentages of surface area exposed to normal impingement, oblique impingement, and parallel flow. (Hereafter, the third factor will be referred to as the 'normal surface area exposure'.) It is proposed that these three factors are the primary mechanisms through which fin arrays affect the average heat transfer coefficient for impinging air jets.

The significance of the normal surface area exposure arises from the following: in terms of heat transfer, normal impingement is superior to oblique impingement, and oblique impingement is superior to parallel flow. In the stagnation zone, the smooth surface is exposed to normal impingement with its associated high heat transfer characteristics. While the fins increase the total surface area, there is no additional normal surface area exposure in the stagnation zone. Generally, the additional surface area is exposed to either oblique impingement or parallel flow. Indeed, for the pyramidal fin system, the normal surface area in the stagnation zone has been replaced entirely by oblique impingement area. Table 1 shows these percentages for the stagnation zone of the pyramidal and short, intermediate, and tall square fins.

The data of Fig. 4 are useful in evaluating the $\overline{Nu}$ dependence on fin type seen in Fig. 3 in terms of the turbulence level and fluid velocity. The figure shows the radial component of average air velocity ($\bar{u}/V$) and normalized r.m.s. turbulent fluctuations (u'/V) as a function of height (y) at a radial position one jet diameter from the test surface perimeter for the surfaces modified with the pyramidal, tall square, intermediate square, and short square fins and for the smooth surface. Although these results clearly do not represent the entire flow field (since $\bar{u}/V$ and u'/V will depend on the measurement position around the periphery of the heater), they do provide insight into the mechanisms by which the fins affect $\overline{Nu}$ for impinging jets with modified surfaces. Figure 4(a) reveals that the addition of surface modifications results in an increase in the average radial velocity, a phenomenon which may be termed 'flow channeling'. The increased mean velocities are more likely to yield higher average heat transfer coefficients in the flow

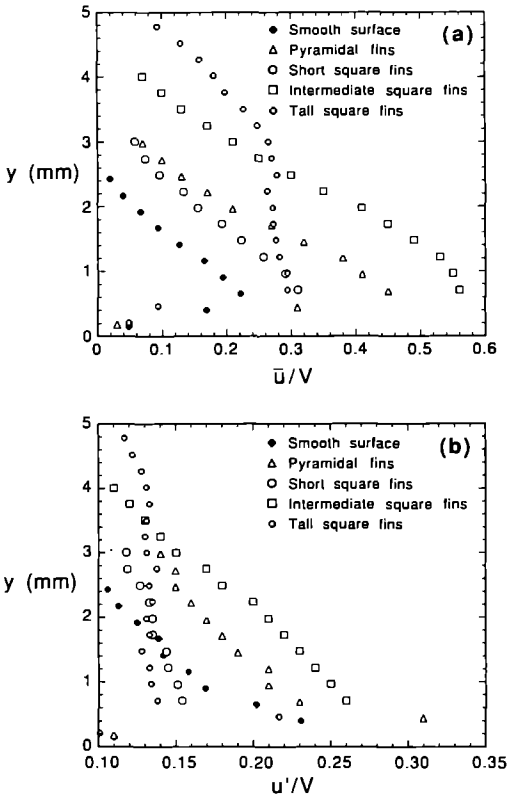

FIG. 4. Average radial velocity and r.m.s. turbulence as a function of distance from the base, $d = 6.91$, $z/d = 5$, $Re = 14\,100$.

exiting radially from the heater. Interestingly, the structure of the mean radial velocity with height (y) may be loosely correlated with the height of the particular surface modification. Figure 4(b) reveals also that generally higher levels of turbulence are experienced by the four fin systems shown due to the addition of the surface modifications. The combination of flow channeling, increased turbulence, and the normal surface area exposure generally results in a higher average Nusselt number. The effects of the concentric rings and the annular ring surface modifications on turbulence and flow velocity were not investigated. However, since there are no radial flow paths, these extended surfaces have a high potential for flow separation. Both fin geometries are characterized by significantly reduced $\overline{Nu}$, seen in Fig. 3.

Figure 5 shows the overall system effectiveness (ε) as a function of Re for all of the modified surfaces and both nozzle diameters. Recall that the system effectiveness is the ratio of overall heat transfer from the fin/base system to that for the smooth surface at the same Reynolds number and temperature difference. Figure 5 shows that, generally, ε increases with Reynolds number. The effectiveness is greater than unity for all test conditions, indicating an increase in the rate of total heat transfer for all modified surfaces in comparison with the smooth surface.

The dependence of effectiveness on fin type is a function of the three factors given for the $\overline{Nu}$ dependence (level of turbulence, fluid velocity, and normal surface area exposure) and the added effect of the increase in total surface area due to the addition of extended surfaces to a previously smooth surface. As seen in Fig. 5, the effect of the increased surface area is generally more significant in determining the net

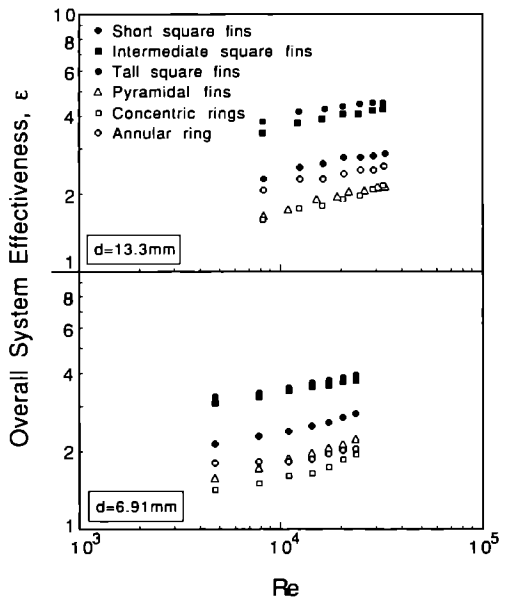

FIG. 5. Overall system effectiveness as a function of Reynolds number for all modified surfaces investigated, $z/d = 5$.

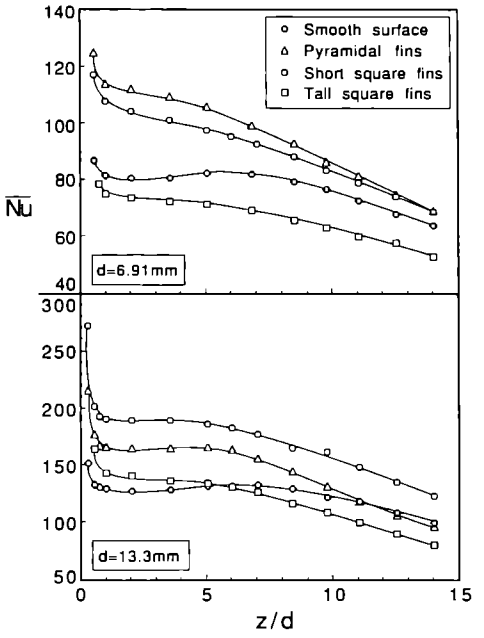

FIG. 6. Average Nusselt number as a function of dimensionless nozzle-to-plate spacing, $d = 6.91$ mm, $Re = 14\,100$, and $d = 13.3$ mm, $Re = 20\,400$.

effect of the fins on the rate of heat transfer than the variations in the average heat transfer coefficient, indicated by $\overline{Nu}$. The tall square fins, which adversely affected $\overline{Nu}$, enhance the heat transfer rate by a factor ranging from approximately 3 to 4. On the other hand, the pyramidal fins, which result in the greatest increase in $\overline{Nu}$, enhance the heat transfer rate by a factor of only 1.5–2. However, the effect of variations in $\overline{Nu}$ is not insignificant; although the intermediate square fins have a smaller increase in the total surface area than the tall square fins, the intermediate fins are nearly as effective as the tall fins due to the significant difference in the average heat transfer coefficient.

Nozzle-to-plate spacing dependence

Figure 6 shows the average Nusselt number as a function of nozzle-to-plate spacing for the surfaces modified with the pyramidal, short square, and tall square fins as well as the smooth surface. Figure 7 is a similar plot of the overall system effectiveness. The faired curves through the data are shown to facilitate comparison of the test surfaces.

It is beneficial to analyze the smooth surface results for later comparison with the modified surfaces. In the potential core region ($1 < z/d < 6$), the jet core velocity remains relatively unchanged, while the turbulence level increases with increasing z/d. The result is an increase in $\overline{Nu}$ with z/d until the end of the potential core region ($6 < z/d < 7$). In the free jet region ($z/d > 7$), $\overline{Nu}$ decreases with increasing z/d due to a reduction of both the average fluid arrival velocity and the jet turbulence level. The net effect of the poten-

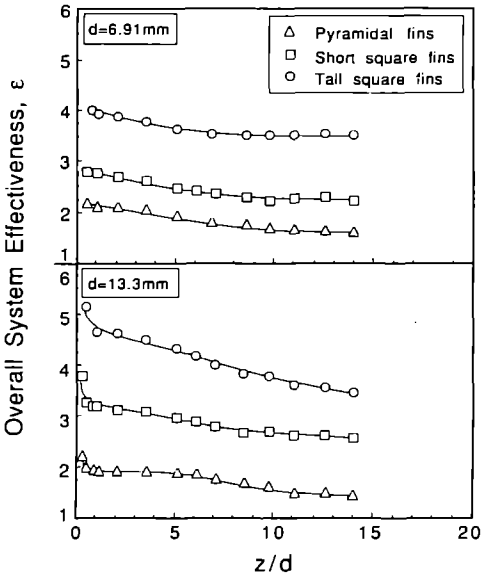

FIG. 7. Dependence of the system effectiveness on nozzle-to-plate spacing, $d = 6.91$ mm, $Re = 14\,100$, and $d = 13.3$ mm, $Re = 20\,400$.

tial core's interaction with the impingement surface is a local maximum in the $\overline{Nu} \sim z/d$ dependence which occurs near $z/d \approx 6$. This has been observed in previous experimental work [13], and is clearly seen in the smooth surface data of the present work (see Fig. 6). In the near surface region ($z/d > 1$), there is a sharp increase in the $\overline{Nu}$ with decreasing z/d due to flow acceleration resulting from the close nozzle-to-plate spacings. All of these trends have been observed previously for smooth, flat surfaces [1, 13, 20].

Figure 6 reveals that the pyramidal fins yield enhanced $\overline{Nu}$ (relative to the smooth surface) over the entire z/d range for both nozzle diameters except at large z/d for the $d = 13.3$ mm diameter nozzle. The short square fins enhance $\overline{Nu}$ for all test conditions. The tall square fins enhance $\overline{Nu}$ with the large nozzle at small z/d (presumably due to increased flow channeling for the tall fins at low z/d), and reduce $\overline{Nu}$ for all other test conditions. The overall system effectiveness, ε, is greater than unity in all cases (Fig. 7). A general decrease in ε with z/d is observed for all of the modified surfaces studied. Note also the dramatic increase in average Nusselt number as $z/d \to 0$. Under these conditions the proximity of the nozzle exit to the top of the extended surfaces causes the flow to accelerate more significantly through the fin channels. Of course, the nozzle could not be positioned at z/d values smaller than that corresponding to the dimensionless height of each fin, H/d, as listed in Fig. 2.

For $z/d > 7$ and $z/d < 1$, the results for the modified surfaces have the same general trends as the smooth surface results. (The acceleration effect for $z/d < 1$ is slightly more pronounced due to flow channeling.) However, in the potential core region ($1 < z/d < 6$), $\overline{Nu}$ for the modified surfaces decreases monotonically with increasing z/d. This is in contrast to the smooth surface behavior, where a local maximum in the heat transfer coefficient at $z/d = 6$ is observed. Evidently, the fins are more effective in the potential core region where the turbulence intensity is otherwise low. Gardon and Akfirat observed a similar result by positioning a turbulence promoting mesh in the jet flow [7]. Figure 7 shows further evidence that the fins are most effective in the potential core region. The dependence of the overall system effectiveness on nozzle-to-plate spacing is stronger in the potential core ($1 < z/d < 6$), as seen by the higher slope of the $\varepsilon \sim z/d$ curve in that region. Indeed, the small diameter nozzle data indicate that ε is nearly independent of z/d at nozzle-to-plate spacings greater than about eight diameters.

Nozzle diameter dependence

As stated previously, two nozzle diameters, $d = 13.3$ and 6.91 mm, were used during the study. In order to analyze the nozzle diameter dependence, the ratio of the average Nusselt number for the large nozzle to that of the small nozzle ($\overline{Nu}_l/\overline{Nu}_s$) was calculated using the $\overline{Nu} = A\,Re^m$ correlations. This ratio is shown in Fig. 8 as a function of Re for the tall square, intermediate square, short square, pyramidal, and smooth surfaces. All of these data were obtained at $z/d = 5$.

As shown by Martin [13], the flow structure as a function of the radial distance from the stagnation point (r) can be divided into two regions: the stagnation flow or impingement region, and the radial flow or wall jet region. Generally speaking, local heat transfer coefficients are higher in the impingement region than in the wall jet region. Thus, average Nusselt numbers typically decrease with increases in R/d. For the two nozzle diameters used here, the large diameter Nusselt number, $\overline{Nu}_l$, corresponds to

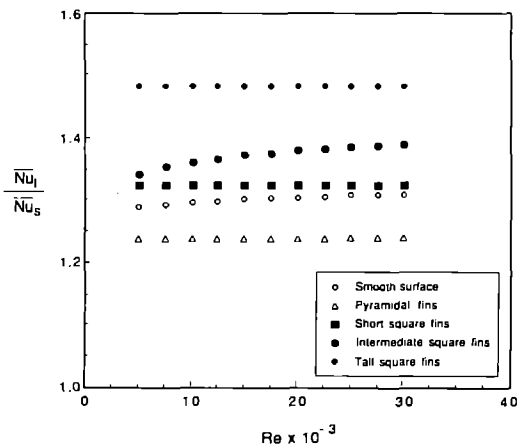

FIG. 8. Ratio of the average Nusselt numbers for the large ($\overline{Nu}_l$) and small ($\overline{Nu}_s$) nozzles as a function of jet Reynolds number, $z/d = 5$.

$R/d = 0.71$, and the small diameter Nusselt number, $\overline{Nu}_s$, corresponds to $R/d = 1.38$. As evident in Fig. 8, $\overline{Nu}_1/\overline{Nu}_s$ is greater than unity for all test surfaces, consistent with the fact that the stagnation region encompasses more of the heater surfaces with the large diameter nozzle.

The ratio $\overline{Nu}_1/\overline{Nu}_s$ is essentially independent of Re. However, $\overline{Nu}_1/\overline{Nu}_s$ does exhibit a fin type dependence. It varies from approximately 1.25 for the pyramidal fins to roughly 1.5 for the tall square fins. For the square fins, $\overline{Nu}_1/\overline{Nu}_s$ increases with fin height. These results indicate that, for square cross-section fins, the fin type dependence may result primarily from channeling effects. Channeling would be greater for the square fins than for the pyramidal fins, and would be expected to increase with fin height. Moreover, the channeling effect would be more pronounced with larger nozzle diameter due to the increased volumetric flow rate for a given Re.

CONCLUSIONS

Experiments were performed to characterize heat transfer to a normally impinging air jet from surfaces modified with fin-type extensions. Six fin geometries were investigated. Heat transfer enhancement was evaluated by comparison with results from a smooth, flat surface. Average Nusselt numbers and system effectiveness have been reported as functions of fin type, jet Reynolds number, nozzle-to-plate spacing, and jet nozzle diameter. The magnitude of the enhancement, as represented by the system effectiveness, was strongly dependent on fin type. The Reynolds number dependence was also significant. To a lesser extent, the system effectiveness exhibited both z/d and R/d dependence. Fin type dependence in the average Nusselt number resulted from variations in (1) the level of turbulence, (2) the fluid velocity at the surface, and (3) the percentages of total fin surface area exposed to normal impingement, oblique impingement, and parallel flow. Unlike jet impingement heat transfer from smooth surfaces, the average Nusselt number for the modified surfaces decreased monotonically with increasing z/d.

Acknowledgements—Financial support of this work under U.S. National Science Foundation Grant CBT-8552493 is gratefully acknowledged.

REFERENCES

1. R. Gardon and J. Cobonpue, Heat transfer between a flat plate and jets of air impinging on it, *Int. Dev. Heat Transfer* 454–460 (1961).
2. S. T. Downs and E. H. James, Jet impingement heat transfer—a literature survey, ASME Paper No. 87-HT-35 (1987).
3. P. Hrycak, Heat transfer and flow rate characteristics of jets impinging on a concave hemispherical plate, *Proc. 7th Int. Heat Transfer Conf.*, Vol. 3, pp. 357–362 (1982).
4. B. R. Hollworth and M. Durbin, Impingement cooling of electronics, *Natn. Heat Transfer Conf.*, HTD-Vol. 111, pp. 89–96 (1989).
5. T. T. Hamadah, Air jet impingement cooling of an array of simulated electronics packages, *Proc. 1989 Natn. Heat Transfer Conf.*, HTD-Vol. 111, pp. 97–105 (1989).
6. C. D. Donaldson, R. S. Snedeker and D. P. Margolis, A study of free jet impingement—Part II. Free jet turbulent structure and impingement heat transfer, *J. Fluid Mech.* **45**, 477–512 (1971).
7. R. Gardon and J. C. Akfirat, The role of turbulence in determining the heat transfer characteristics of impinging jets, *Int. J. Heat Mass Transfer* **8**, 1261–1272 (1965).
8. G. I. Gorshkov, Near-wall turbulence in jet impingement on a wall, *J. Appl. Mech. Tech. Phys.* **25**, 233–241 (1984).
9. K. Kataoka and T. Mizushina, Local enhancement of the rate of heat transfer in an impinging round jet by free-stream turbulence, *Proc. 5th Int. Heat Transfer Conf.*, Vol. 2, Paper FC8.3, pp. 305–309 (1974).
10. K. Kataoka, M. Suguro, H. Degawa, K. Maruo and I. Mihata, The effect of surface renewal due to large-scale eddies on jet impingement heat transfer, *Int. J. Heat Mass Transfer* **30**, 559–567 (1987).
11. C. O. Popiel and O. Trass, The effect of ordered structure of turbulence on momentum, heat and mass transfer of impinging round jets, *Proc. 7th Int. Heat Transfer Conf.*, Vol. 6, pp. 141–146 (1982).
12. J. N. B. Livingood and P. Hrycak, Impingement heat transfer from turbulent air jets to flat plates—a literature survey, NASA TM X-2778 (1973).
13. H. Martin, Heat and mass transfer between impinging gas jets and solid surfaces. In *Advances in Heat Transfer*, Vol. 13, pp. 1–60. Academic Press, New York (1977).
14. P. Hrycak, Heat transfer from impinging jets—a literature review, AFWAL-TR-81-3504, Flight Dynamics Laboratory, Wright-Patterson AFB, Ohio (1981).
15. M. M. Ali Khan, N. Kasagi, M. Hirata and N. Nishiwaki, Heat transfer augmentation in an axisymmetric impinging jet, *Proc. 7th Int. Heat Transfer Conf.*, Paper FC6.3, pp. 363–368 (1982).
16. P. Hrycak, Heat transfer from impinging jets to a flat plate with conical and ring protuberances, *Int. J. Heat Mass Transfer* **27**, 2145–2154 (1984).
17. N. T. Obot and T. A. Trabold, Impingement heat transfer within arrays of circular jets: Part II—effects of cross-flow in the presence of roughness elements, *Trans. ASME, J. Turbomachinery* **109**, 594–601 (1987).
18. R. V. Fleishman and W. W. Yuen, Mesh enhanced forced convection heat transfer for high heat flux applications, *Proc. 1988 Natn. Heat Transfer Conf.* (Edited by H. R. Jacobs), Vol. 1, pp. 653–660. ASME, New York (1988).
19. T. G. Beckwith, N. L. Buck and R. D. Marangoni, *Mechanical Measurements* (3rd Edn). Addison-Wesley, Reading, Massachusetts (1982).
20. D. Lytle and B. W. Webb, Secondary maxima for air jet impingement at low nozzle-to-plate spacings, *Proc. Second World Conf. on Experimental Heat Transfer, Fluid Mechanics, and Thermodynamics* (Edited by J. F. Keffer, R. K. Shah and E. N. Gánic), pp. 776–783. Elsevier, New York (1991).